Scattering, loss, and gain of surface plasmons

Beijnum, F. van

Quasi-cylindrical wave contribution in experiments on extraordinary optical transmission

A metal film perforated by a regular array of subwavelength holes exhibits an unexpectedly large transmission at particular wavelengths, named the extraordinary optical transmission (EOT) of metal hole arrays [28]. EOT was first attributed to surface plasmon polaritons (SPP), reawakening a large interest in plasmonics [39–41] and subwavelength metallic surfaces [30, 42, 43]. Experiments soon revealed that the field diffracted at a hole or slit is not a SPP mode alone [34]. Further theoretical analysis [36] predicted that the extra contribution, the quasi-cylindrical wave (CW) [35, 44–46], impacts the EOT phenomenon too. In this chapter, we experimentally demonstrate the relative importance of the SPP and CW in EOT by considering hole arrays of different hole densities. From the measured spectra we extract microscopic scattering parameters, which allow us to evidence that the CW only impacts the EOT for high densities, when the hole spacing is roughly one wavelength. Besides providing a deeper understanding of the EOT and the related Wood's anomaly, the extraction of microscopic scattering parameters from the measurement of macroscopic optical properties paves the way towards novel design strategies.

F. van Beijnum, C. Rétif, C. B. Smiet, H. T. Liu, P. Lalanne, and M. P. van Exter, Nature **492**, 411 (2012).

2.1 Introduction

Understanding the EOT quantitatively has been a major challenge in the past decade (see ref. [43] for a review). An important contribution to EOT may be the quasi-cylindrical wave (CW), which is the field on the metal surface diffracted at a subwavelength indentation, in addition to the surface plasmon contribution [35, 44, 46]. The justification to separate these two field contributions lies in the fact that the CW also exists in the absence of surface plasmons, namely in the case of a perfect electric conductor interface [35, 45, 47], and for a dielectric interface [48]. For the perfect electric conductor, the CW is nothing else than a cylindrical wave in free space with a $x^{-1/2}$ decay rate. For metals of finite conductivity at optical frequencies, the cylindrical behavior is only seen in the vicinity of the indentation, at a few wavelengths distance. At larger distances, the CW decay rate keeps on increasing gradually until it reaches an asymptotic algebraic value ($x^{-3/2}$) at large distances. Because of the periodicity of hole arrays, all these decay rates are simultaneously present in the EOT phenomenon.

Another important result in the understanding of EOT is the development of a semi-analytic SPP model, that quantifies the SPP contribution to EOT. This microscopic model relies on scattering parameters that describe the interaction between light and the holes. The microscopic model correctly predicts the EOT lineshape, but underestimates the magnitude of the transmission by roughly a factor two for visible frequencies. These results suggest that the SPP is only responsible for roughly half of the EOT phenomenon [36], whereas the other half is due to the CW. So far, this interpretation is purely theoretical and remains conceptual and we are not aware of any experimental confirmation yet. The reason is probably that many scattering parameters in the model are dispersive and had to be calculated using complicated simulations [36]. Measuring all these parameters with sufficient accuracy is a tremendous experimental issue that we challenge here.

In this chapter, we provide a direct evidence for the respective role of SPP and CW in the EOT, by exploiting the fact that the SPP and CW have different characteristic damping lengths. This is achieved by measuring the transmission spectra of a series of hole arrays with varying hole density, designed to resonate at the same near-infrared frequency (≈ 750 nm). We find that the normalized transmission peaks of all the low-density arrays are virtually identical. The largest density array, which corresponds to the classical hole array in [28], has a hole spacing that corresponds to the CW damping length of one wavelength. This array shows a sudden boost of the normalized transmission compared to the transmission of the other arrays. The observa-

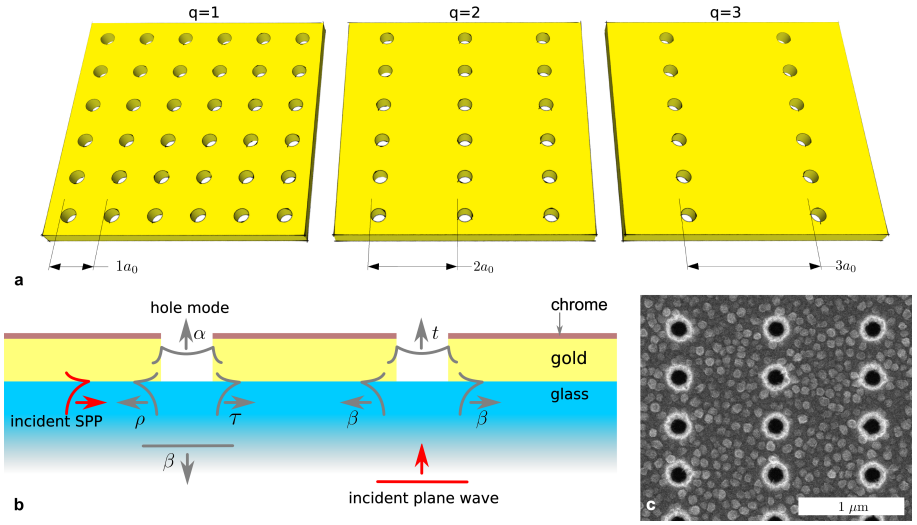

Figure 2.1: An illustration of our sample design. To demonstrate a quasi-cylindrical wave contribution to EOT, we compare the transmission of a series of hole arrays with different densities that all resonate at the same wavelength. **a,** To decrease the hole density, the distance between so-called hole chains is increased. **b,** The relevant scattering processes are sketched. At the left hole there is a surface plasmon incident (red arrow) that is either transmitted (τ), reflected (ρ), coupled into the hole (α) or to free space (β). At the right hole a free space mode is incident (red arrow), which scatters to a surface plasmon (β) or couples into the hole (t). **c,** A scanning electron microscope picture of the $q = 2$ hole array.

tion of this atypical behavior for the largest density array constitutes a direct proof of the embodiment of the CW in the EOT, or more generally of the CW in phenomena related to subwavelength metallic gratings.

2.2 Experiments

Figure 2.1 illustrates how we vary the hole density: we increase the distance between so-called hole chains, while keeping the properties of these chains fixed. The holes within the chains are spaced by $a_y = a_0 = 450$ nm. The distance between the chains is chosen to be $a_x = qa_0$, where q=1, 2, 3, 4, 6, and 7. The holes perforate two metal layers: a 150 nm gold layer that is deposited on a glass substrate, and a 20 nm chromium layer that damps the SPP at the air interface. We measured the zeroth order transmission spectra of each array using x-polarized light, hence SPP propagating along the y-axis are negligible [10, 36, 49, 50].

Figure 2.2 shows the measured spectra on a semilog scale. Each array has a transmission peak between 735 and 775 nm, which shifts to shorter wavelengths as the hole spacing increases. The transmission minima of these resonances are at 724 ± 4 nm, which is very close to the expected value of $\mathrm{Re}\, n_{\mathrm{eff}} a_0 = 729$ nm, where n_{eff} is the ratio between the SPP wave vector and

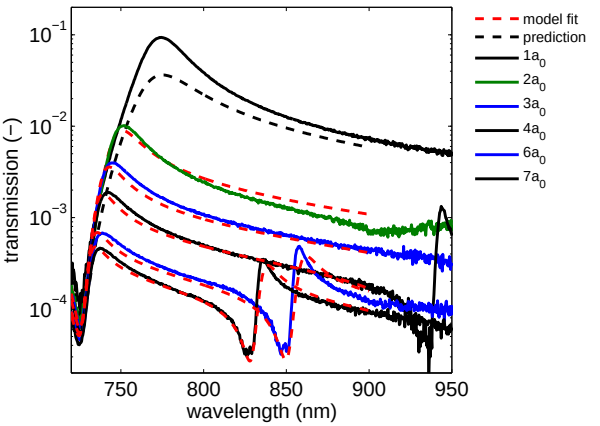

Figure 2.2: Measured transmission spectra (solid curves) and the fitted surface plasmon model (red dashed curves). Each dashed curve has the same parameters except for the q-value. The parameters are based on a fit of Eq. (2.3) to the data of arrays with $q \geq 2$. The black dashed curve is a model prediction, plotting Eq. (2.3) with the same parameters as the other curves but with $q = 1$. The model accurately predicts all maxima and minima of the measured data for $q \geq 2$, showing that the transmission of these arrays is dominated by surface plasmons.

the free space wave vector [51, 52]. The magnitude of the transmission minima ranges between 0.6×10^{-4} and 2×10^{-4}. The resonance peaks are the result of a surface wave propagating in the x-direction, with the number of oscillations per lattice period equal to the q-value of the hole array. For the 4, 6, and $7a_0$ arrays additional resonances are also visible between 800 and 1000 nm. These resonances correspond to a surface wave propagating in the x-direction with q-1 oscillations per period.

As evidenced by the log-scale plots, the zeroth order transmission dramatically decreases as the hole density decreases. As will be justified hereafter, it essentially scales as $1/q^2$. Thus in Fig. 2.3, we plot $q^2\times$transmission on a linear scale, for $q = 1$, 2, 4, and 6. The results for $q = 3$ and $q = 7$ have been removed for clarity of the figure. By plotting the data on a linear scale we see that the scaled transmission is almost constant when going from $q = 2$ to $q = 6$. However for $q = 1$, the transmission peak is markedly larger, more than two times larger than all the other peaks. The fact that all the arrays except $q = 1$ virtually exhibit identical extraordinary transmission peaks is not fortuitous and, as will be interpreted hereafter, it reveals the resonant transmission due to SPPs only. With this respect, the sudden and marked increase of the peak transmission for the largest density ($q = 1$) constitutes an important result of the present work: it is a direct signature of the additional short-range contribution of the CW to EOT.

The previous conclusions are inferred qualitatively on the basis of the difference in damping lengths between SPP and CW. Helped by the microscopic SPP model in ref. [36], we will now aim at providing a fully quantitative analysis of the data in Figs. 2.2 and 2.3 to explicitly support our conclusions. The major drawback of the microscopic approach is that it requires the knowledge

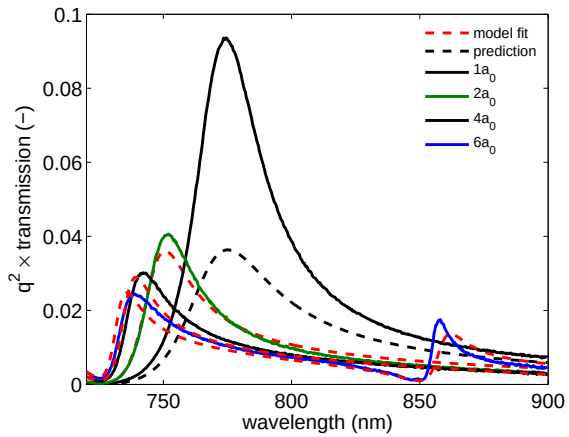

Figure 2.3: By plotting $q^2 \times$ transmission, it is shown that there is a sudden increase of the transmission when comparing the $q = 1$ array to the other arrays. By plotting the SPP model too, we show that this behavior is not predicted by considering surface plasmons alone.

of many dispersive complex-valued parameters, which need to be calculated using full-vectorial simulations at every wavelength. This precludes its direct application to analyze experimental data. Hereafter, we revisit the model in depth and show that an analytical expression involving only five independent real non-dispersive fitted parameters may accurately reproduce the whole set of experimental spectra in Fig. 2.2 for $q \geq 2$, but produces wrong predictions for the case $q = 1$.

2.3 Simplifying the microscopic model

The microscopic model, as originally formulated in [36], considers one-dimensional hole chains (along the y-direction) as the elementary scatterers of the hole arrays and assumes that the electromagnetic interaction between the hole chains is mediated only by the SPP modes on unperturbed interfaces, the CW being totally neglected. The microscopic model couples three modes: the SPP mode at the gold-glass interface that consists of SPP propagating in both directions along the x-axis, the fundamental mode within the holes, and the free space modes.

The modes are coupled by the following scattering parameters, illustrated in Fig. 2.1b. An incident surface plasmon can: couple into the holes of the hole chain (α); couple to free space (β); or be transmitted (τ) or reflected (ρ). An incident plane wave can couple to a surface plasmon (β) or directly into the holes of the hole chain (t). The propagation of the surface plasmon from one hole chain to another is described by $e^{-ik_{\mathrm{spp}}a_x}$, where $k_{\mathrm{spp}} = 2\pi n_{\mathrm{eff}}/\lambda$ is the wave vector of the SPP on a flat gold-glass interface and a_x is the distance between the hole chains. Because we kept the hole size constant for each array, the scattering parameters ($\alpha, \beta, \rho,$ and τ) should be the same for each array.

Only the hole spacing a_x depends on the parameter q, namely $a_x = qa_0$.

In line with the coupled mode approach proposed in [36] we derived (see appendix) the transmission coefficient t_f of a single hole chain, modified by the SPP excited at the surrounding hole chains:

$$t_f = t + \frac{2\alpha\beta}{e^{-ik_{\mathrm{spp}}a_x} - (\rho + \tau)}. \tag{2.1}$$

The assumption that the hole chains only excite a plane SPP wave in the x-direction is valid if the incident polarization is along the x-axis. Moreover, the holes within the hole chain have to be less than a SPP wavelength apart [36]. The model neglects the influence of the metal-air interface. In the appendix we show this assumption holds if the surface plasmons at that interface are sufficiently damped by the chromium layer.

The optical transmission measured at a particular angle is a sum of the field contributions from all illuminated hole chains. If we define N_0 as the number of illuminated hole chains for the $q = 1$ array, $N = N_0/q$ is the number of hole chains as a function of q. In the zeroth diffraction order, the contributions from all hole chains are in phase, hence the transmitted intensity is [53]

$$T \propto 1/q^2 \left| t_f \right|^2, \tag{2.2}$$

where the proportionality factor is independent of q, as further discussed in the appendix.

Equations (2.1) and (2.2) are not yet simple enough to be used for modeling experimental data. Its six parameters are complex, so we have twelve real-valued parameters. To reduce the number of free parameters we combine both $\alpha\beta$ and $\rho + \tau$ into one complex parameter each. Furthermore, we need only the phase difference between t and $\alpha\beta$. For the complex variable k_{spp} we combine linearly interpolated literature values for the gold properties [54] with a measured value of the index of refraction of the substrate (1.51). This leaves us with a model of five free parameters.

Another crucial step towards fitting the model to the data is the wavelength dependence of the parameters. The following approximations are used: 1) $t \propto \lambda^{-2}$, as indicated by several studies [43, 55–57]; 2) $\alpha\beta \propto \lambda^{-4}$ in rough agreement with a factor 4 reduction for a wavelength increase of 38%, as reported in ref. [36]; 3) we keep $\rho + \tau$ constant, as calculations show that this sum has limited dispersion; 4) the phase of $\rho + \tau$ and the phase difference between $\alpha\beta$ and t are also kept constant with wavelength. So finally, we have the following fit equation:

$$T = q^{-2} \left| \frac{\lambda_0^2}{\lambda^2} p_1 + \frac{\lambda_0^4}{\lambda^4} \frac{p_2 e^{ip_3}}{e^{-ik_{\mathrm{spp}}qa_0} - p_4 e^{ip_5}} \right|^2. \tag{2.3}$$

Parameter	Fit value	Error
p_1	0.0740	0.0006
p_2	0.0243	0.0006
p_3	0.681π	0.013π
p_4	0.857	0.009
p_5	0.132π	0.006π
$\left\lvert e^{-ik_{\mathrm{spp}}a_0}\right\rvert$	1.021	N.A.

Table 2.1: The values of the fitting parameters p_1 to p_5. For completeness we also give the absolute value of $e^{-ik_{\mathrm{spp}}a_0}$, evaluated at 800 nm. Also we give an estimate of the error in the fit values.

with $\lambda_0 = 800$ nm and p_1 to p_5 the five real-valued parameters in the model. The physical significance of parameters p_1 and p_4 is discussed in the appendix.

2.4 Fitting the microscopic model to the transmission spectra

The fitted curves obtained with the model are shown with the red dashed curves in Fig. 2.2. For the fit we only use the data of arrays $q = 2$ to $q = 7$, as we expect the transmission of these arrays to be dominated by SPP. To make sure that the minima are fitted well, we fitted $^{10}\log(\text{data})$ to $^{10}\log(\text{model})$. The result is plotted in Fig. 2.2 on a logarithmic scale, and the fit values are given in Table 2.1. For the arrays with q=2, 3, 4, 6, 7 the model describes the spectral positions of all minima and maxima very accurately, including the $(q-1,0)$ resonances. Also the transmission magnitude is well modeled.

Remarkably too, Eq. (2.3) used with $q = 1$ (black dashed curve in Figs. 2.2 and 2.3) fails at predicting the experimental data for $q = 1$. In particular it underestimates the transmission peak by a factor 2.5. The latter is consistent with the theoretical predictions in [36], which conclude that SPP account for only half of the total transmitted energy at peak transmittance for a resonance wavelength of 700nm. In the Appendix, we expand the SPP microscopic model to incorporate the CW (see Eq. (2.7) therein), this extended model accurately describes the experimental data for $q = 1$ (see Fig. 2.6). Let us emphasize that this result is achieved using the exact same scattering parameters and does not require any additional fitting.

The observation that the transmission spectra of these six different hole arrays (including the particular $q = 1$ case) can be described with only five parameters is a big success of the microscopic theory. Moreover, it is of importance that these parameters are directly related to elementary scattering processes. Apparently the resonance of perforated metal surface can be modeled with a combination of a SPP mode and a CW on an unperturbed surface and a few extra scattering parameters, which can be inferred from simple transmission measurements.

2.5 Conclusion

We have presented the first experiments that quantitatively show the respective contributions of surface plasmons polaritons (SPP) and the quasi-cylindrical wave to extraordinary optical transmission (EOT). This in-depth analysis has been made possible by deriving the elementary scattering parameters defined in [36] from classical transmission measurements performed on a series of hole arrays. The possibility of making these microscopic scattering parameters experimentally accessible may be paramount for understanding and designing complex periodic or aperiodic metallic structures. Hence, variations to this modeling approach may have important implications in applying plasmonic structures to sensors, photovoltaics, LEDs or lasers.

2.6 Methods

The sample is fabricated as follows. Using e-beam lithography we created pillars on a glass substrate. Then we deposited 150 nm of gold and subsequently deposited the 20 nm chromium. Finally, we etched away the pillars. The function of the chromium layer is to heavily damp surface plasmons on the gold-air interface. We analyzed scanning electron microscope pictures of each array to conclude that the average hole radius is 81 ± 4 nm. By studying the position of the diffraction orders using a 635 nm laser diode, we concluded that the lattice parameters a_0 of all arrays are equal within 2 nm. Each array covers an area of 400 μm $\times$ 400 μm.

The transmission spectrum of each array is measured using the following setup (not shown). The light of a halogen lamp is filtered (longpass, 600 nm) and coupled into a 200 μm diameter fiber. The light coupled out of the fiber is polarized along the x-axis. The end facet of the fiber is imaged onto the sample with a magnification of 1.5. The 300 μm diameter spot is centered on the 400 μm $\times$ 400 μm arrays. The zeroth order transmission is imaged (M=2/3) onto a 365 μm diameter fiber that leads to an Ocean Optics 2000+ USB spectrometer. To measure the reference spectrum, we move the sample out of the beam using a stage.

An accurate measurement of the transmission spectrum requires sufficient spatial and temporal coherence of the illuminating and detected light. The spatial coherence at the sample is ensured by the limited numerical aperture (NA $\approx (6 \pm 2) \times 10^{-3}$) of the illumination, which corresponds to a coherence length of a few tens of micrometers on the sample [53], being much larger than an SPP propagation length. The temporal coherence is ensured by the spectral resolution of the detecting spectrometer. The 1 nm resolution corresponds to coherence times of hundreds of femtoseconds [53] and is an order of magnitude better then strictly needed.

Appendix

In this appendix, we provide the equations of the SPP model [36] and of the SPP+CW model [45] that are used for fitting the experimental data. We also explain the fitting process in more detail.

For the 2D hole arrays considered in the experiment, the transmission coefficient t_F of the zeroth-order plane wave can be expressed with a Fabry-Perot equation [36],

$$t_F = \frac{t_A t'_A e^{ik_0 n_{FM} d}}{1 - r_A r'_A e^{i2k_0 n_{FM} d}} \tag{2.4}$$

for which we assume that the transmission of light is mediated by the least-attenuated fundamental mode of subwavelength holes. In Eq. (2.4), t_A and r_A (resp. t'_A and r'_A) are the transmission and reflection coefficients of the fundamental mode at the gold-glass (respectively chromium-air) interface, as defined in Fig. 2.4, n_{FM} is the complex effective index of the fundamental mode, d is the thickness of gold film and $k_0 = 2\pi/\lambda$. Then the zeroth-order power transmittance is $T = (n_g/n_a)\,|t_F|^2$, where $n_g = 1.5$ and $n_a = 1$ are the refractive indices of glass and air, respectively. In the absence of surface-wave-mediated resonance at the air interface, due to the damping chromium layer, t'_A and r'_A depend only weakly on the wavelength in the spectral range of interest (essentially fixed by the resonance of the glass interface), and $|r'_A| << 1$ [36, 58]. Thus Eq. (2.4) can be simplified as:

$$t_F = t_A t'_A e^{ik_0 n_{FM} d} \tag{2.5}$$

in which the sole resonance term is t_A. Within the scope of the pure-SPP model, which assumes that only SPPs are carrying energy between the hole

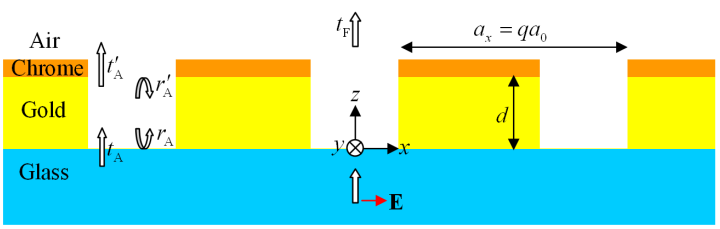

Figure 2.4: Scattering parameters t_F, t_A, t'_A, r_A and r'_A defined for a 2D hole array. The x-polarized plane wave (sketched by the vertical arrow in glass region) is normally incident from the glass side in the experiment. The array periods in x- and y-directions are qa_0 and a_0 respectively, and the gold film thickness is d. t_F is the transmission coefficient of the zeroth-order plane wave, t_A (resp. t'_A) is the transmission coefficient from the incident plane wave to the transmitted fundamental mode of the hole array at the gold-glass interface (resp. from the fundamental mode to the transmitted zeroth-order plane wave at the gold-chromium-air interface), and r_A (resp. r'_A) is the reflection coefficient of the fundamental mode at the gold-glass (resp. gold-chromium-air) interface.

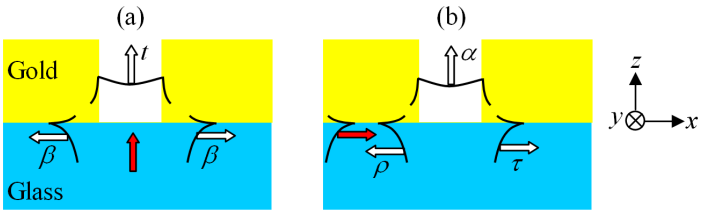

Figure 2.5: SPP-scattering parameters t,α,β, ρ and τ defined for a single y-periodic chain of holes. **a,** For an incident plane wave (sketched by the red arrow in glass region), t is the transmission coefficient from the plane wave to the fundamental hole-chain mode, and β is the SPP launching coefficient (sketched by the horizontal arrows). **b,** For an incident SPP (red arrow), ρ and τ are the reflection and transmission SPP coefficients, and α is the coupling coefficient to the fundamental hole-chain mode.

chains at the glass interface [36], t_A under normal incidence can be expressed as

$$t_A = t + \frac{2\alpha\beta}{u^{-1} - (\rho + \tau)}. \tag{2.6}$$

where $u = e^{ik_{\mathrm{spp}}qa_0}$ is the phase shift experienced by the SPP in one period qa_0; t,α,β, ρ and τ are SPP-scattering parameters associated to the scattering of SPPs by individual hole chains (see Fig. 2.5 for a definition and [36] for more details), t corresponds to the direct transmission, β denotes the SPP launching coefficient, α describes the coupling from the excited SPP to the fundamental chain mode, and ρ and τ characterize the in-plane reflection and transmission of the SPP. The pure-SPP model and the associated Eq. (2.6) are used for fitting the transmission spectra and for obtaining the red dash-dotted curve in Fig. 2.2.

Recently, two of the authors have extended the pure-SPP coupled-wave model by incorporating the contribution of the CW to the transmission. Importantly, it is found that the scattering coefficients associated to the CW are (in the limit of small apertures) strictly identical to the SPP scattering coefficients α, β, ρ and τ, and that a coupled-wave model considering both the SPP and quasi-cylindrical wave can thus be straightforwardly deduced from the pure SPP model. Details concerning the derivation can be found in [45]. In the generalized SPP+CW (Hybrid Wave, or HW) model, which is considering the total field on the interface and which is therefore much more accurate, the refined "equivalent" of Eq. (2.6) is

$$t_A = t + \frac{2\alpha\beta}{(1/\sum H_{HW} + 1) - (\rho + \tau)}. \tag{2.7}$$

where $\sum H_{HW} = \sum H_{SPP} + H_{CW}$ combines a SPP part, $\sum H_{SPP} = 1/(u^{-1} -$

1), and a CW part, $\sum H_{CW}$, which represents a lattice summation of CW field at multiples of period qa_0 ($\sum H_{CW}$ is known analytically [45]).

As explained in the main text, with the SPP model the zeroth-order power transmittance T for our samples with periods qa_0 and a_0 can be expressed with a fitting-ready form deduced from Eq. (2.6),

$$T(q) = q^{-2} \left| t_{fit} + \frac{2\alpha_{fit}}{u(q)^{-1} - (\rho_{fit})} \right|^2 . \tag{2.8}$$

where $t_{fit} = tt'_{A,fit}$, $\alpha_{fit} = 2\alpha\beta t'_{A,fit}$, $t'_{A,fit} = e^{ik_0 n_{FM} d}\sqrt{n_g/n_a}t'_A$. Equation (2.8) exhibits an analytical dependence of T with q, in which the complex fitted parameters t_{fit}, α_{fit} and ρ_{fit} are all independent of q, and $u^{-1}(q) = e^{ik_{\mathrm{spp}}qa_0}$ is known. This enables a unified theoretical framework for analyzing samples with the same metal thickness, hole size and periodicity a_0 along the y-direction but with different periods in the x-direction (as done in Fig. 2.2 in the main text for q=2-7).

As indicated in the main text, the wavelength dependence of t_{fit}, α_{fit} and ρ_{fit} are adopted to be $t_{fit} = p_1(\lambda_0/\lambda)^2$, $\alpha_{fit} = p_2 e^{ip_3}(\lambda_0/\lambda)^4$ and $\rho_{fit} = p_4 e^{ip_5}$, where the real quantities p_1 to p_5 are independent of the wavelength. Thus on overall, the whole series of experimental spectra obtained for various q's (this represents a large quantity of data) are fitted with only five real parameters. The drastic reduction in the parameter space not only evidences that the microscopic model captures the essence of the physical mechanism of the EOT, but also allows for a very robust fitting procedure.

For the SPP+CW model, Eq. (2.8) becomes,

$$T(q) = q^{-2} \left| t_{fit} + \frac{2\alpha_{fit}}{1/\sum H_{HW}(q) - (\rho_{fit})} \right|^2 . \tag{2.9}$$

where $H_{HW}(q)$ depends on q in a known analytical way [45]. Therefore once the unknown quantities t_{fit}, α_{fit} and ρ_{fit} are determined by the previous fitting procedure, the prediction of the SPP+CW model is immediately computed with the fitted quantities; no additional fitting or numerical calculations are required. In Fig. 2.6, we show the results of the SPP+CW model for $q = 1$ (see the red sold curves). On the logarithmic scale the deviations between the model and the data are similar to that of the other samples for $q = 2 - 7$. On the linear scale it is clearly seen that the CW boosts the transmission by more than a factor two. The small deviations between experiment and the SPP model for $q = 2 - 7$ or the SPP+CW model for $q = 1$ are probably due to the many approximations we had to make to derive our fit expression.

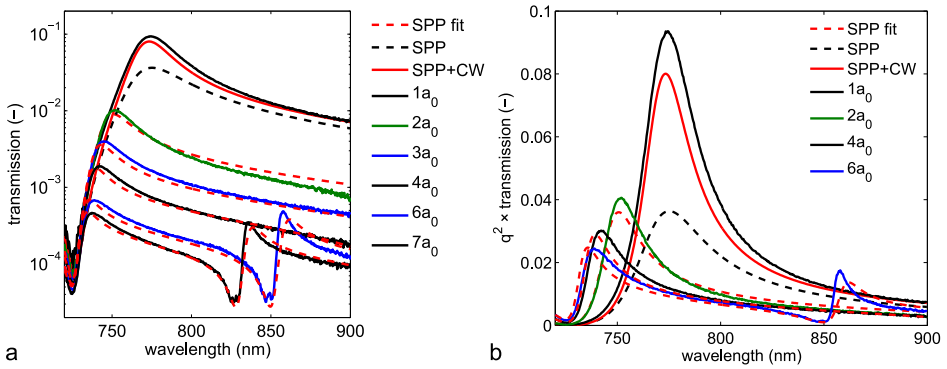

Figure 2.6: Results of the SPP model and the SPP+CW model using the fit parameters from the SPP model. **a,** On a logarithmic scale it is seen that the SPP+CW model fits the $q = 1$ data for well over three orders of magnitude. **b,** By plotting $q^2\times$transmission on a linear scale, we show that the predicted transmission for the SPP+CW model is more than two times larger than for the SPP model. This shows that the CW explains the discrepancy between the SPP model and the experimental data.

Also, we fit the data on a logarithmic scale, and therefore the fit routine allows some deviations at the maximum transmission, in favor for a better fit of the minima. We believe that the remarkable agreement obtained for $q = 1$ in Fig. 2.6 between the experimental data and the SPP+CW model and not for the pure-SPP model constitutes a critical proof of the embodiment of the quasi-cylindrical wave in the EOT.

Finally, we would like to discuss the physical significance of two of our fit parameters. The parameter p_1 allows us to calculate the transmission enhancement and suppression, as this parameter characterizes the light that is transmitted without surface wave resonance. Given the fitted $p_1^2 = 5.5 \times 10^{-3}$, the maximum transmission of 0.093 for $q = 1$ is 17 times larger than this value, while the minimum of 8.5×10^{-5} is 65 times smaller. For the $q = 6$ sample, the enhancement and suppression are reduced because of SPP absorption and the virtual absence of the CW. The enhancement is now 4.4, while suppression is reduced to a factor 3.3.

A second interesting fit parameter is $p_4 = |\rho+\tau|$. This parameter quantifies the scattering losses of the SPP wave at the hole chains. Its fit value of $p_4 = 0.857$ should be compared with the modulus of $e^{ik_{\mathrm{spp}}a_0} = 0.98$ around the resonance wavelength. This comparison shows that the SPP scattering losses are roughly 7 times larger than the absorption losses for our densest ($q = 1$) sample, while they are approximately equal for the $q = 7$ low-density sample.